

PAPER

# Advanced adhesion and friction measurement system

To cite this article: Meng Li *et al* 2017 *Meas. Sci. Technol.* **28** 035601

View the [article online](#) for updates and enhancements.

## Related content

- [Recent advances in the surface forces apparatus \(SFA\) technique](#)  
J Israelachvili, Y Min, M Akbulut *et al.*
- [Role of adhesion in shear strength of nanowire-substrate interfaces](#)  
M P Manoharan and M A Haque
- [Force calibration in lateral force microscopy: a review of the experimental methods](#)  
Martin Munz

## Recent citations

- [Controlled support of a magnetic fluid at a superhydrophobic interface](#)  
Qingwen Dai *et al*
- [A Hybrid Two-Axis Force Sensor for the Mesoscopic Structural Superlubricity Studies](#)  
Sun *et al*
- [Effects of bulk viscoelasticity and surface wetting on the contact and adhesive properties of a soft material](#)  
Meng Li *et al*

# Advanced adhesion and friction measurement system

Meng Li<sup>1</sup>, Wei Huang<sup>1,2</sup> and Xiaolei Wang<sup>1,2</sup>

<sup>1</sup> College of Mechanical and Electrical Engineering, Nanjing University of Aeronautics and Astronautics, Nanjing 210016, People's Republic of China

<sup>2</sup> Jiangsu Key Laboratory of Precision and Micro-Manufacturing Technology, Nanjing 210016, People's Republic of China

E-mail: [wxl@nuaa.edu.cn](mailto:wxl@nuaa.edu.cn)

Received 19 December 2016

Accepted for publication 9 January 2017


Published 2 February 2017



## Abstract

An advanced micro-force tester for investigating the micromechanical behavior of various patterned surfaces in dry and wet conditions is presented in this paper. The parallel slice-beam configuration of the tester not only eliminates the large load-dependent slope and tangential displacement at the free end that is found in a single beam system, but also performs a trans-scale deflection with high sensitivity and linearity for force sensing. Meanwhile, the simple structure is characterized by low cost, high efficiency, and ease of fabrication. An integrated nano- and micro-stage comprise the mobile table to produce a large stroke with high resolution, which is specifically required in wet adhesion testing because of the formation of a long liquid bridge. Preliminary experiments of adhesion and friction conducted using PDMS pillars with a plano-convex lens validated the feasibility of this setup.

Keywords: adhesion, friction, micro-force tester, slope angle, double parallel cantilever beam

 Supplementary material for this article is available [online](#)

(Some figures may appear in colour only in the online journal)

## 1. Introduction

Nature provides largely appealing surfaces and mechanisms that are regarded as precious resources to inspire people to design new machines. Geckos can quickly climb uneven and rough walls, even while upside down, by utilizing the seta on their feet [1, 2]. Tree frogs and newts can attach to wet slippery leaves or rocks without falling through use of their patterned toe pads [3–8]. The scientific mechanisms of strong adhesion associated with high friction include van der Waals forces, capillary forces, electrostatic attraction, and suction [9–15]. To investigate these micromechanical behaviors, a convenient and precise micro-force tester would be highly valuable. In previous years, various apparatuses have been developed to accurately characterize the adhesion and friction of a surface. The surface force apparatus (SFA), a typical surface force measurement instrument primarily used for nano-tribology, rheological systems, and various material testing, employs a thin cantilever to accurately measure the nano-sized

intermolecular forces on a thin film or mica surface by fringes of equal chromatic order (FECO) [16, 17]. Another widely used micro-force tester is the micro-tribometer, which was initially designed for micro- or nano-tribology, and is often constructed by the researchers themselves [18–21]. For this type of tester, the sensitive element is an elaborate double-leaf spring whose deflection can be captured by a fiber optic sensor to obtain the normal load and frictional force during measurement. In addition, a simple but convenient 2D force transducer consisting of two independent cantilever beams and strain gauges is also often used in bionic surface studies [10, 13, 22]. For a single cantilever beam, a large slope angle at the free end is always generated under a small load, which is undesirable in indentation or flat-flat adhesion experiments. To address this issue, these test structures have been further improved by researchers through implementing a symmetric design, for example Kroner *et al* utilizing a double-clamped glass beam for the adhesion test on bioinspired fibrillary [23–26] and Varenberg *et al* employing a symmetric four-leaf

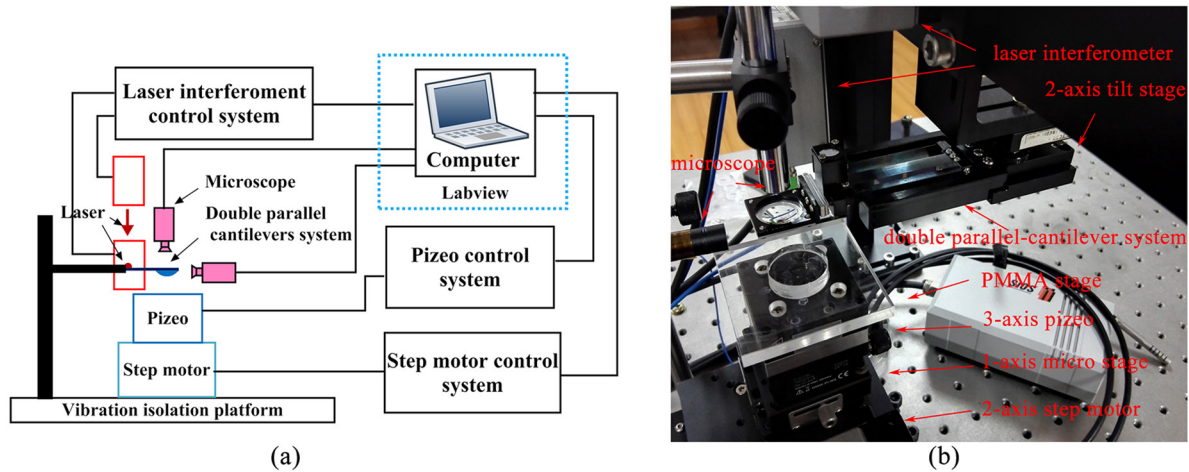


Figure 1. (a) Schematic and (b) photograph of the adhesion and friction tester.

spring for flat-on-flat micro-force testing [14, 27, 28]. To this end, a well-designed spring beam is the key component in a force sensor, which is responsible for the performance of the whole test system.

For a micro-force test on a micro-patterned surface, it is generally accepted that the more patterns a probe contacts, the better is its response, the more drastically a force acts, and the more reliable the results are. However, patterns ranging from several nanometers to hundreds of micrometers are all available in present scientific investigations, exhibiting a multi-scale phenomenon. To perform tests on these patterns, in addition to avoiding production of a large load-dependent slope, an ample indenting area achieved by a large-sized probe and a sufficient range of force sensing by the spring beam, up to two or three orders of magnitude, are also essential. Although the previous symmetric designs have the ability to deal with flat-on-flat in dry tests, these setups may still suffer from some drawbacks, especially for wet adhesion tests. For example, the hypersensitive arm of four-leaf spring, which is usually comprised of a material with low elasticity such as glass or steel, may be too delicate to deflect to the required extent or support a large-sized probe. Meanwhile, their circuitous narrow constructions are also difficult to machine with high precision on a pony-sized scale. The double-clamped glass beam is simple, robust and effective, but it may be hard to extend with a friction test module. Furthermore, in wet adhesion, another multi-scale phenomenon occurs in which in order to accurately preload, the resolution of the mobile table must be nano-scale, but the slender liquid bridge, sticking to the probe, deforms on a millimeter scale in an indentation or detachment event. As a result, the current moving tables that are driven by just a single piezo are ineffective during the measurement process. Worst of all, in previous studies, the design of the stiffness and structure of the spring beams used was not described in detail and only the final results were provided, thereby making the beams highly difficult for novices to reproduce.

In this work, a setup was designed to overcome these limitations with a cleverly constructed spring beam and an integrated mobile table. The design principles of the spring beam stiffness, the ganged operation of the mobile table, and the implementation of the whole system have been described in

detail in the following sections. To verify the feasibility of test construction, preliminary tests of adhesion and friction were also conducted using PDMS pillars.

## 2. Methods

### 2.1. Design index and description of the set-up

The objective of this work was to develop a test system with a small terminal slope angle ( $\ll 0.01^\circ$ ), high force resolution ( $\ll \text{mN}$  range), high force measurement range ( $>$ three orders of magnitude), highly linear spring constants (the standard deviation of fitting line  $< 0.1\%$ ), and *in situ* visualization. To achieve these goals, two key components were improved in this setup. First, inspired by the SFA and weighing sensor [16, 29], the sensitive beam system was designed using two groups of slice-beams in a parallel configuration, where the parallelogram distorted law was adopted to eliminate the terminal slope angle. Because it is difficult to use a flat probe for a friction test on very soft material because of its deep indentation at the contact boundary, a large curvature lens was used. Moreover, a combined table of a nano- and a micro-stage was used. The linkage of these two stages enabled the table to both accurately locate and produce a large stroke.

Figure 1 shows the schematic and picture of the test system. The sensitive beam was fixed on a 2-axis tilt stage (Lianyi, China) to achieve horizontal alignment. For force sensing, a two-dimension laser interferometer (SP2000, SIOS Messtechnik, Germany) with a resolution of 20 pm was mounted on an aluminum alloy rack to measure cantilever deflection. The probe at the free end of cantilever beams was a plano-convex lens with a curve radius of 18.5 mm (Purshee Experiment, China), Young's modulus of  $7.2 \times 10^{11}$  Pa, and Poisson's ratio of 0.2, and the reflector was fabricated using two mirrors coated with an Al film (Laiengao, China) mounted on a cube. The nano-stage was a piezo (P-611.3, Physik Instrumente, Germany) with a resolution of 0.2 nm and range of 100  $\mu\text{m}$ , and the micro-stage was comprised of a step motor (Lianyi, China) with a resolution of 2.5  $\mu\text{m}$  and range of 20 mm. In addition, a 1-axis micro stage (Lianyi, China) was used for auxiliary adjustment of the specimen's position.

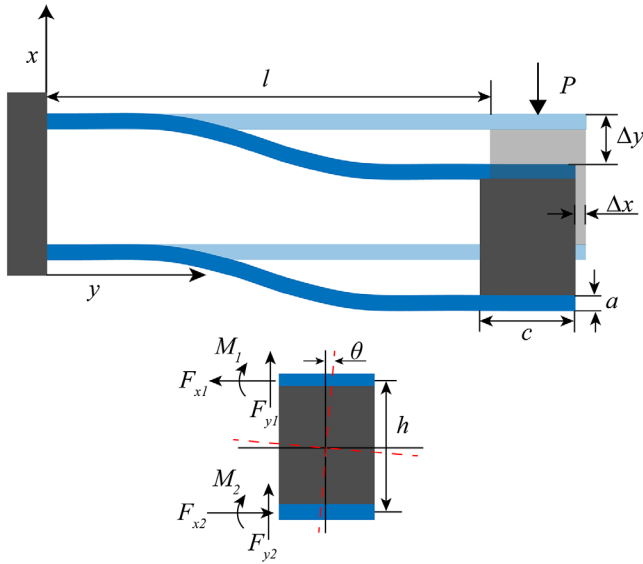


**Figure 2.** Schematic of a double parallel cantilever beam.

In the monitoring system, two microscopes placed on the side view and top view of the probe were used for real-time visualization, and environmental data, such as temperature, air pressure, and humidity were also recorded by sensors during testing. The whole setup was mounted on an active anti-vibration table. To acquire the test data and connect these independent commercial units, a new program was developed using Labview software.

## 2.2. Design of the sensitive beam and performance analysis

Regarding force measurements, if a single cantilever beam is used as the only force sensor, it is unavoidably accompanied by a free-end load-dependent slope. To eliminate this problem, a symmetric construction or a double parallel cantilever beam may be used as alternatives. Figure 2 shows the deflection of the double parallel cantilever beam selected for this study under normal load  $P$ . In this configuration, one end of the beam is tied to the free end of the lens probe, and the other end is connected to a rigid substrate. The material, geometry, and dimensions of the two cantilevers were identical, and their working length was  $l$ . In order to acquire the beam's properties, a mechanical mode was established. The equilibrium equation could be described as follows:

$$F_{y1} + F_{y2} - P = 0 \quad (1)$$

$$F_{x1} - F_{x2} = 0 \quad (2)$$

$$F_{x1} \frac{h+a}{2} + F_{x2} \frac{h+a}{2} = M_1 + M_2 + F_{y2} \frac{c}{2} + F_{y1} \frac{c}{2} \quad (3)$$

where  $h$  is the space between the two parallel cantilevers,  $a$  is the thickness of the lamellar beam,  $c$  is the length of the link block at the free end,  $F_{y1}$ ,  $F_{y2}$ ,  $F_{x1}$ ,  $F_{x2}$  are the internal forces, and  $M_1$ ,  $M_2$  are moments of the beam.

Considering the geometry, the equation of deformation compatibility was given by

$$\Delta l = \theta \frac{h+a}{2} \quad (4)$$

where  $\Delta l$  is the elongation (or shortening) distance of the cantilevers and  $\theta$  is the slope angle.

From mechanics of materials [30], the deflection  $\Delta y$ , slope angle  $\theta$ , and elongation  $\Delta l$  of a single cantilever beam under the normal load, bending moment, and axial force could be obtained by applying the superposition principle. Then, at  $x = l$ ,  $\Delta y$ ,  $\theta$ , and  $\Delta l$  could be solved by equations (2)–(4). Hence,  $\theta(x)$  and  $\Delta y(x)$  could be expressed as

$$\theta(x) = \frac{Px}{2EI} \left( l - \frac{x}{2} - \frac{A(h+a)^2 l - 4Ic}{2(4I + A(h+a)^2)} \right), 0 \leq x \leq l \quad (5)$$

$$\Delta y(x) = \frac{Px^2}{4EI} \left( l - \frac{x}{3} - \frac{A(h+a)^2 l - 4Ic}{2(4I + A(h+a)^2)} \right), 0 \leq x \leq l \quad (6)$$

where  $E$  is the Young's modulus,  $I$  is the moment of inertia, and  $A$  is the cross-sectional area of cantilever beam. Here, the cross section of the cantilever beam was rectangular with a width of  $b$ , such that the moment of inertia and cross-section could be described as  $I = \frac{ba^3}{12}$ ,  $A = ba$ . Therefore, equations (5) and (6), and the horizontal movement  $\Delta x$ , at  $x = l$ , could be written as

$$\theta = \frac{Pl(l+c)}{Eba \left( \frac{a^3}{3} + (h+a)^2 \right)} \quad (7)$$

$$\Delta y = \frac{Pl^3}{2Eba^3} \left( 1 + \frac{1 + \frac{c}{l}}{\frac{1}{3} + \left( \frac{h}{a} + 1 \right)^2} \right) \quad (8)$$

$$\Delta x = l - \int_0^l \cos(\theta(x)) dx \quad (9)$$

Finally, the stiffness of double parallel cantilever beam  $K$  could be written as

$$K = \frac{P}{\Delta y} = \frac{2Eba^3}{l^3} \left( 1 - \frac{1 + \frac{c}{l}}{\frac{4}{3} + \left( \frac{h}{a} + 1 \right)^2 + \frac{c}{l}} \right) \quad (10)$$

and, the slope angle  $\theta$  at the free end could be written as

$$\theta = \frac{2(l+c)P}{KI \left( \frac{4}{3}l + \left( \frac{h}{a} + 1 \right)^2 l + c \right)} \quad (11)$$

However, since  $\cos(\theta(x))$  is a non-integral function, equation (9) could not be solved directly. So, the numerical method was used and  $\Delta x$  was expressed as

$$\Delta x = l - \sum_{i=1}^n \cos \left( \theta \left( \frac{il}{n} \right) \right) \frac{l}{n} \quad (12)$$

It is well known that there is an ideal stiffness of the spring beam for the system to perform accurate measurements. If equipped with a lower stiffness, the spring beam is too

**Table 1.** Description of spring beams used.

Parameters	$a$ (mm)	$b$ (mm)	$c$ (mm)	$l$ (mm)	$h$ (mm)	$E$ (MPa)
Vertical beams	0.3	8	5	50	8	$1.9 \times 10^5$
Horizontal beams	0.3	10	5	45	24	$1.9 \times 10^5$

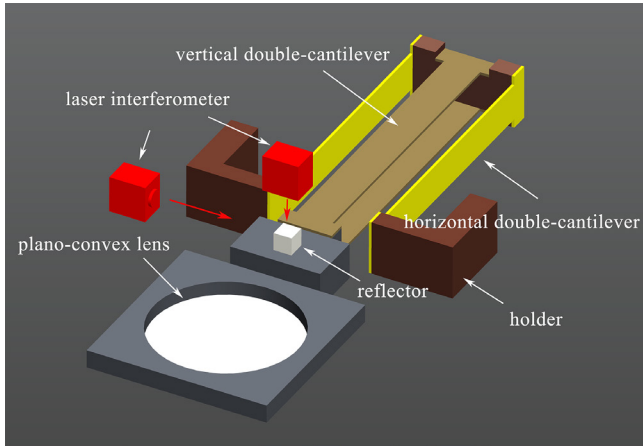


**Figure 3.** The construction of the double parallel cantilever beam system.

delicate, thereby restricting the measurement range and size of the probe; in contrast, excessive stiffness results in poor sensitivity. Consulting previous studies, we initially used vertical and horizontal stiffness values of  $600 \text{ N m}^{-1}$  and  $1000 \text{ N m}^{-1}$ , respectively. From an economic and feasible machining perspective, a spring steel 65Mn, with good elastic properties, was selected for this study. All parameters of the spring beams are shown in table 1. According to equation (10),  $K_v$  and  $K_h$  were  $655.7 \text{ N m}^{-1}$  and  $1124.9 \text{ N m}^{-1}$ , respectively. The construction of the sensitive beam is shown in figure 3. Four slice-beams were divided into two groups of parallel configurations by the link block and holder for measuring adhesion and frictional force. Compared with current spring beams, this decentralized structure is simple, convenient, and economic.

Figure 4(a) shows the deflection of the vertical beam axis under different loads according to equations (5) and (6) and table 1. It can be seen that along most points of the beam, the deflection and slope angle both increased significantly with increasing load, except at the fixed end,  $x = 0$ , whose value was always zero. When under a certain load, the deflection increased along the axis and reached a maximum value at the free end of the cantilever,  $x = l$ . However, for the slope angle of the beam, the derivative of deflection could be well described as a quadratic function curve as shown in figure 4(b). Around the midpoint, the beam distorted acutely, but the free end, nearly a zero-point with a negligible slope angle, demonstrated a nearly parallel translation. Furthermore, the feasibility of indentation studies has been verified in figure 4(c) by equation (12) and Hertz theory. Though the terminal tangential displacement increased with the increasing load, it could be negated when compared with the magnitude of the indentation depth under an applied load. Especially in typical

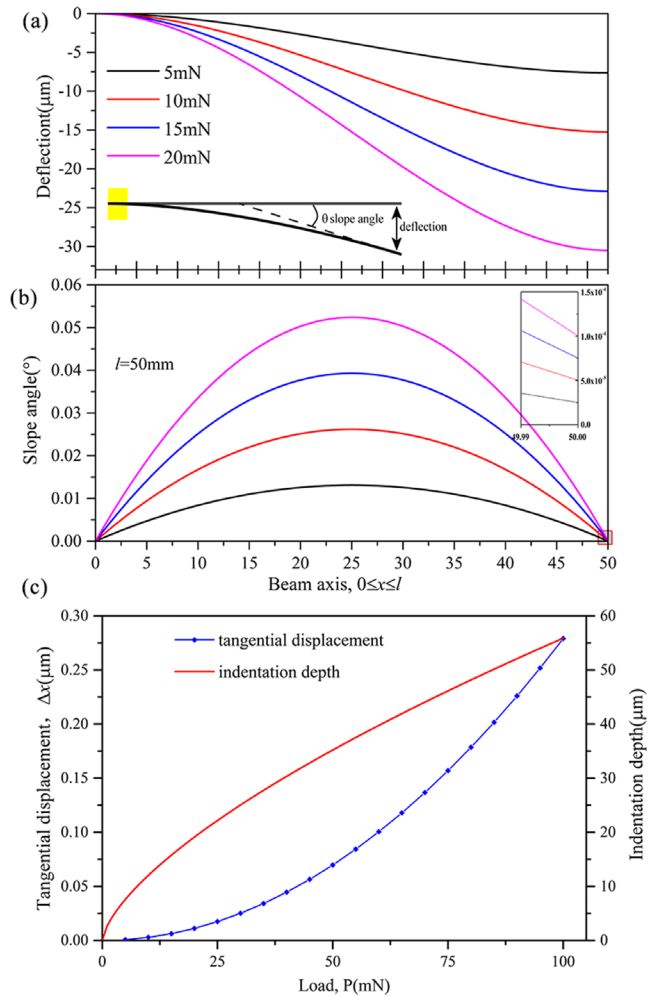


**Figure 4.** (a) Deflections, (b) slope angles of vertical beams and tangential displacement of its free end.

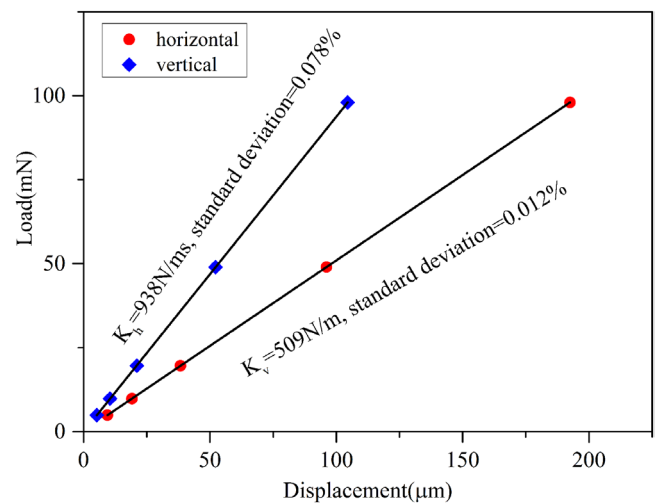


**Figure 5.** Calibration of horizontal ( $K_h$ ) and vertical ( $K_v$ ) cantilever stiffness. Solid lines are fitted linearly.

indentation studies the results are more obvious owing to the conehead or pinhead shape instead of the large curvature lens.

The vertical and horizontal stiffness of cantilevers were determined by hanging precise weights from the probe end and recording the resulting deflection. In the case of

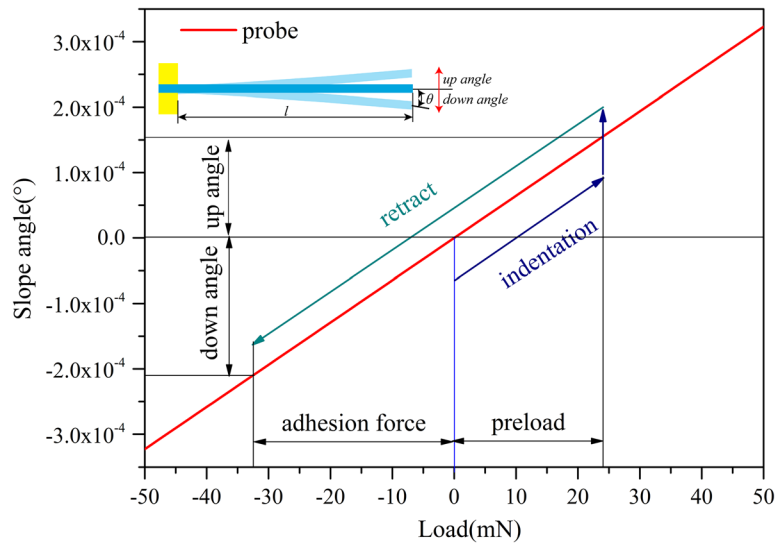


Figure 6. Slope angles of the probe in indentation and retraction.

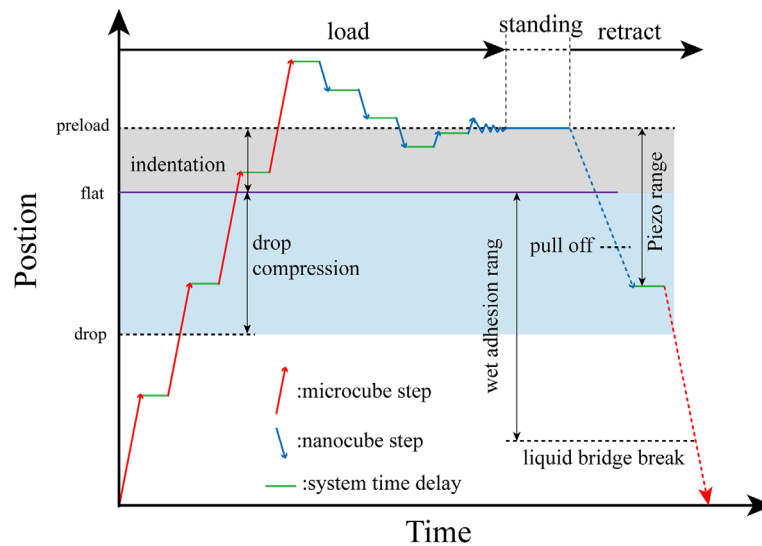
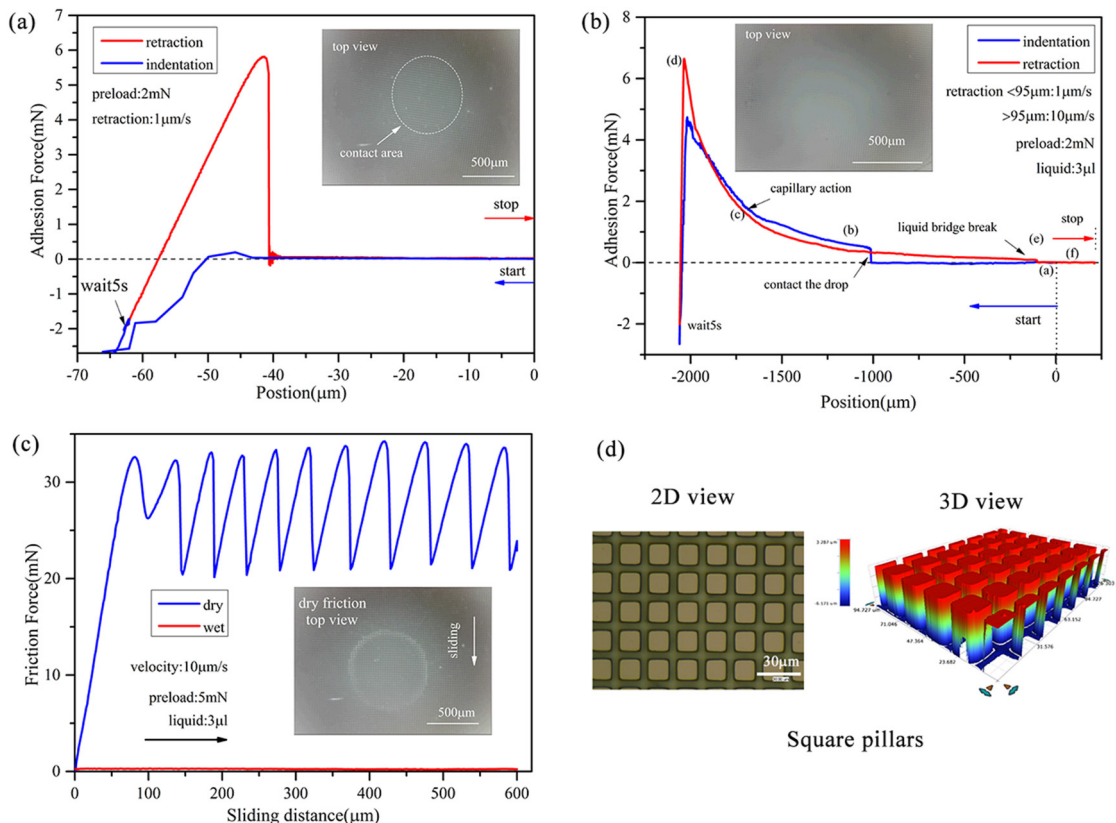


Figure 7. Illustration of the wet adhesion test process by the mobile table.

the horizontal calibration, the entire cantilever system was rotated  $90^\circ$  by a fixture so that a hanging weight would generate horizontal deflection. Figure 5 shows that a linear relationship between the deflection and the force was obtained for both the vertical and horizontal directions. Using these fitted lines (standard deviation:  $1.22 \times 10^{-2}\%$  lateral and  $7.8 \times 10^{-2}\%$  normal), the vertical and horizontal stiffness values were computed to be  $509 \text{ N m}^{-1}$  and  $938 \text{ N m}^{-1}$ , respectively. In contrast to the theoretical results, the generated differences were probably caused by the bolt-on connection, rather than the rigid coupling, in addition to the machining errors. A typical adhesion test process is illustrated in figure 6 by using equation (11) with  $K_v = 509 \text{ N m}^{-1}$ . The results further present the relatively small slope angles in indentation and retraction. Therefore, the free end of the spring beam could be regarded as performing a vertically oriented parallel translation in the  $z$ -direction during measurements.

### 2.3. The ganged operation of the integrated mobile table

In order to avoid the shortcomings of a narrow range or low precision resulting from using a single nano- or micro-stage, an integrated mobile table was utilized. Figure 7 presents the loading and retracting process of the mobile table in a typical wet adhesion measurement test. First, the step motor moved to the target position in micro steps. When the probe contacted the drop placed on the micro-patterned surface, it compressed causing a liquid bridge to form. Subsequently, to achieve a preload, the probe induced an indentation upon the specimen. In this process, the nano-stage iteratively moved in nano-scale steps towards the preload, finally converging at a high-precision position. After the standing time, the piezo first retracted at a speed of  $\geq 1 \text{ nm s}^{-1}$  to conduct the detachment event slowly, overcoming van der Waals and capillary forces. When moving over the piezo range, the step motor launched at a speed of  $\geq 1 \text{ } \mu\text{m s}^{-1}$ , and the liquid bridge



**Figure 8.** Typical tests of pillars performed in dry and wet condition. (a) and (b) Pull-off force curves, (c) friction curves, (d) microscope images of pillars with length 15 μm, gap 5 μm and height 8.5 μm.

force between the probe and specimen acted independently until breaking.

### 3. Results and discussion

Figure 8(a) shows a typical force-displacement curve of the adhesion tested on square pillars, shown in figure 8(d), in dry conditions. As shown in figure 3, during the preload, the indentation iterated in micro-steps and converged to the target in nano-steps, so substantial standing time to reach equilibrium was necessary. Here, that time was 5 s. It can be seen that a clear pull-off event was detected during the retraction process. The maximum force at the detachment event, which occurred drastically and suddenly, yielded an adhesive force value of approximately 5.8 mN. In that event, the interaction of the dry adhesion was simple, mainly consisting of van der Waals forces, and its distance was also very short, approximately 22 μm for the pillars. However, a vast difference was observed in the wet adhesion because of the strong capillary effects, as shown in figure 8(b). For hydrophilic regime, 1% (w/w in distilled water, surface tension  $32.69 \pm 0.47 \text{ mN m}^{-1}$ ) sodium dodecyl sulfate (SDS) was employed in tests. The indentation curve shows that the contact of the drop and probe produced a considerable liquid bridge force by capillary action. Similarly, in the retraction after standing time, a significant bonding characteristic of the liquid bridge also produced a pull-off force of approximately 6.7 mN at the same preload, larger than the

dry condition. Moreover, the detachment curve was smooth and gradually fell towards zero until the liquid bridge broke. Compared to the dry adhesion, the interaction of detachment in the wet case was moderate and lengthy, resulting in a distance of about 1970 μm, an increase of nearly 90 fold. To examine the behavior of the liquid bridge in the wet adhesion, images of the side views of the experiments were recorded. Photographs from the microscope during wet adhesion are shown in figure 9, illustrating the approach (a), compression of the drop (b), indentation (c), retraction (d), maximum liquid bridge length (e), and liquid bridge breaking (f). These photographs are also marked in figure 8(b) and demonstrate good fitness with the measured curves. Figure 8(c) shows the friction curves obtained on square pillars. The difference in sliding behavior of the wet and dry surfaces is obvious. The dry surface exhibited a pronounced stick–slip motion with a large frictional force, while the wet surface presented stable undisturbed sliding with a small frictional force. The presence of liquid, which was introduced into the contact as a lubricant, was most likely responsible for this phenomenon, changing the frictional behavior of the surface. These results of adhesion and friction measured on pillars in dry and wet conditions were consistent with those of previous studies [7, 13, 14, 31–33]. (Typical real-time visualizations of tests were shown in supplementary material [stacks.iop.org/MST/28/035601/mmedia](http://stacks.iop.org/MST/28/035601/mmedia).)

By theoretical analysis and experimental testing, this advanced setup features the following specifications—sensitive

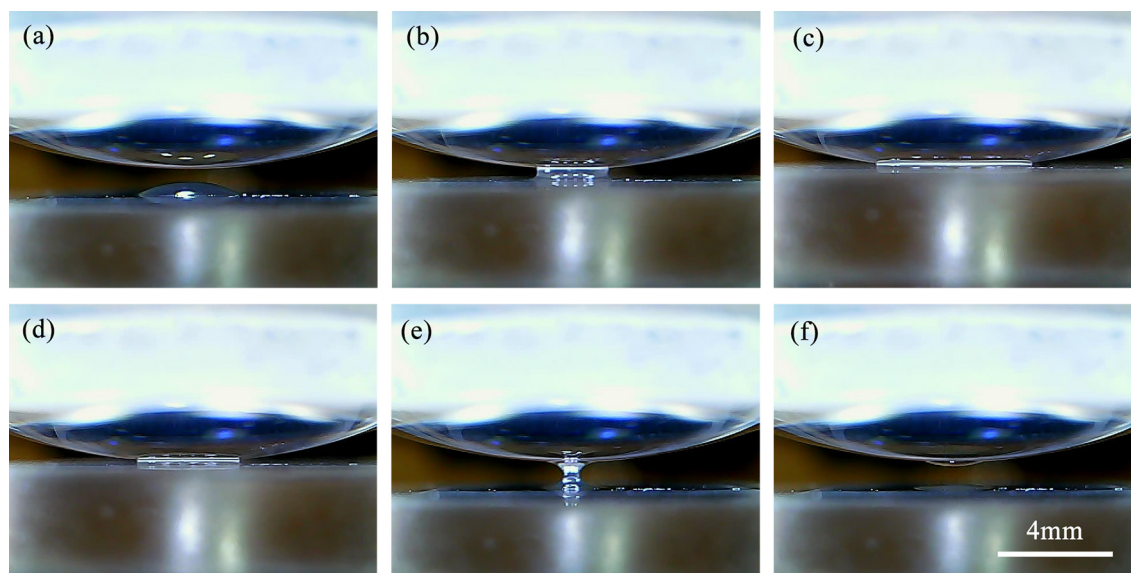


**Figure 9.** Side-view images from a wet adhesion experiment. (a) Approach, (b) compressing the drop, (c) indentation, (d) retraction, (e) maximum liquid bridge length, and (f) liquid bridge break.

beam deflection  $\leq \pm 800 \mu\text{m}$  (with high elasticity reaching up to mm, although a conservative value was selected with consideration for changes in the laser intensity); low noise  $\leq \pm 60 \text{nm}$ ; terminal tangential displacement  $\leq 0.28 \mu\text{m}$ , and a slope angle  $\leq (6.4 \times 10^{-4})^\circ$  when the preload  $\leq 100 \text{mN}$  in the vertical direction; platform migration length  $\leq 20 \text{mm}$  with a resolution of  $0.001 \mu\text{m}$ .

#### 4. Conclusion

In this study, we developed an effective micro-tribometer structure employing a double parallel cantilever beam configuration and an integrated mobile stage to overcome the multi-scale problems in wet adhesion measurements. The performance analysis indicated that this double parallel cantilever beam system, similar to a symmetric structure, effectively overcomes the limitations associated with large slope and tangential displacement at the free end, and exhibits high sensitivity and linearity during large-scale deformation, thereby achieving the initial design goals. Furthermore, this decentralized structure is characterized by low cost, simplicity, and ease of fabrication. Moreover, the ganged operation of piezo and step motor achieves an improved travel with high precision for the wet adhesion tests. The results of the preliminary tests in a pillars/glass tribopair confirmed these efficiencies. Therefore, this advanced tester has sufficient competence for characterizing surface properties on patterns by friction, adhesion, and indentation. Additionally, the detailed and systematic design process of the spring beams in this work can be regarded as a guide to make further improvements or design new testers in other research.

#### Acknowledgments

This research was supported by the National Nature Science Foundation of China (NSFC) (Grant No. 51675268).

#### References

- [1] Autumn K, Liang Y A, Hsieh S T, Zesch W, Chan W P, Kenny T W, Fearing R and Full R J 2000 Adhesive force of a single gecko foot-hair *Nature* **405** 681–5
- [2] Autumn K and Peattie A M 2002 Mechanisms of adhesion in geckos *Integr. Comp. Biol.* **42** 1081–90
- [3] Federle W, Barnes W J, Baumgartner W, Drechsler P and Smith J M 2006 Wet but not slippery: boundary friction in tree frog adhesive toe pads *J. R. Soc. Interface* **3** 689–97
- [4] Barnes W J P 2007 Functional morphology and design constraints of smooth adhesive pads *MRS Bull.* **32** 479–85
- [5] Scholz I, Barnes W J, Smith J M and Baumgartner W 2009 Ultrastructure and physical properties of an adhesive surface, the toe pad epithelium of the tree frog, *Litoria caerulea* white *J. Exp. Biol.* **212** 155–62
- [6] Huang W and Wang X L 2013 Biomimetic design of elastomer surface pattern for friction control under wet conditions *Bioinspir. Biomim.* **8** 046001
- [7] Li M, Huang W and Wang X 2015 Bioinspired, peg-studded hexagonal patterns for wetting and friction *Biointerphases* **10** 031008
- [8] Wang S, Li M, Huang W and Wang X 2016 Sticking/climbing ability and morphology studies of the toe pads of Chinese fire belly newt *J. Bionic Eng.* **13** 115–23
- [9] Autumn K, Sitti M, Liang Y A, Peattie A M, Hansen W R, Sponberg S, Kenny T W, Fearing R, Israelachvili J N and Full R J 2002 Evidence for van der Waals adhesion in gecko setae *Proc. Natl Acad. Sci. USA* **99** 12252–6
- [10] Drechsler P and Federle W 2006 Biomechanics of smooth adhesive pads in insects: influence of tarsal secretion on attachment performance *J. Comp. Physiol. A* **192** 1213–22
- [11] Gorb S N 2008 Biological attachment devices: exploring nature's diversity for biomimetics *Phil. Trans. R. Soc. A* **366** 1557–74
- [12] Varenberg M and Gorb S N 2008 A beetle-inspired solution for underwater adhesion *J. R. Soc. Interface* **5** 383–5
- [13] Drotlef D M, Stepien L, Kappl M, Barnes W J P, Butt H J and del Campo A 2013 Insights into the adhesive mechanisms of tree frogs using artificial mimics *Adv. Funct. Mater.* **23** 1137–46
- [14] Varenberg M and Gorb S N 2009 Hexagonal surface micropattern for dry and wet friction *Adv. Mater.* **21** 483–6



- [15] Iturri J, Xue L, Kappl M, García-Fernández L, Barnes W J P, Butt H J and del Campo A 2015 Torrent frog-inspired adhesives: attachment to flooded surfaces *Adv. Funct. Mater.* **25** 1499–505
- [16] Israelachvili J *et al* 2010 Recent advances in the surface forces apparatus (SFA) technique *Rep. Prog. Phys.* **73** 036601
- [17] Benz M, Chen N and Israelachvili J 2004 Lubrication and wear properties of grafted polyelectrolytes, hyaluronan and hylan, measured in the surface forces apparatus *J. Biomed. Mater. Res. A* **71** 6–15
- [18] Liu Y, Gubisch M, Hild W, Scherge M, Spiess L, Knedlik C and Schaefer J A 2005 Nanoscale multilayer WC/C coatings developed for nanopositioning, part II: friction and wear *Thin Solid Films* **488** 140–8
- [19] Liu Y, Liu S, Hild W, Luo J and Schaefer J A 2006 Friction and adhesion in boundary lubrication measured by microtribometers *Tribol. Int.* **39** 1674–81
- [20] Tomala A, Werner W S M, Gebeshuber I C, Dörr N and Störi H 2009 Tribochemistry of monomolecular lubricant films of ethanolamine oligomers *Tribol. Int.* **42** 1513–8
- [21] Scherge M and Gorb S S 2001 *Biological Micro- and Nanotribology* (Berlin: Springer)
- [22] Xue L, Iturri J J, Kappl M, Butt H-J and del Campo A 2014 Bio-inspired orientation dependent friction *Langmuir* **30** 11175–82
- [23] Kroner E, Blau J and Arzt E 2012 Note: an adhesion measurement setup for bioinspired fibrillar surfaces using flat probes *Rev. Sci. Instrum.* **83** 016101
- [24] Micciche M, Arzt E and Kroner E 2014 Single macroscopic pillars as model system for bioinspired adhesives: influence of tip dimension, aspect ratio, and tilt angle *ACS Appl. Mater. Interfaces* **6** 7076–83
- [25] Frensemeier M, Kaiser J S, Frick C P, Schneider A S, Arzt E, Fertig R S and Kroner E 2015 Temperature-induced switchable adhesion using nickel–titanium–polydimethylsiloxane hybrid surfaces *Adv. Funct. Mater.* **25** 3013–21
- [26] Isla P Y and Kroner E 2015 A novel bioinspired switchable adhesive with three distinct adhesive states *Adv. Funct. Mater.* **25** 2444–50
- [27] Varenberg M, Peressadko A, Gorb S N, Arzt E and Mrozek S 2006 Advanced testing of adhesion and friction with a microtribometer *Rev. Sci. Instrum.* **77** 066105
- [28] Heepe L, Varenberg M, Itovich Y and Gorb S N 2011 Suction component in adhesion of mushroom-shaped microstructure *J. R. Soc. Interface* **8** 585–9
- [29] Li C, Wang Y, Wan Z, Chen Y, Xu J-C and Xu X-P 2009 Fiber Bragg grating weighing sensor of beam with two parallel holes *Sensors Actuators A* **154** 12–5
- [30] Gere J M and Goodno B J 1972 *Mechanics of Materials* (New York: Van Nostrand Reinhold)
- [31] Li J, Zhou F and Wang X 2011 Modify the friction between steel ball and PDMS disk under water lubrication by surface texturing *Meccanica* **46** 499–507
- [32] Gorb S N and Varenberg M 2007 Shearing of fibrillar adhesive microstructure: friction and shear-related changes in pull-off force *J. R. Soc. Interface* **4** 721–5
- [33] Tsipenyuk A and Varenberg M 2014 Use of biomimetic hexagonal surface texture in friction against lubricated skin *J. R. Soc. Interface* **11** 20140113